The Magnetic Structure and Electronic Ground States of Mott Insulators GeV_4S_8 and GaV_4S_8

Helen Müller,[†] Winfried Kockelmann,[‡] and Dirk Johrendt*,[†]

Department Chemie und Biochemie, Ludwig-Maximilians-Universität München, Butenandtstrasse 5−13 (Haus D), 81377 München, Germany, and CCLRC Rutherford Appleton Laboratory, Chilton Didcot, Oxfordshire OX11 0QX, United Kingdom

Received December 20, 2005. Revised Manuscript Received February 21, 2006

The ground states of magnetic Mott insulators GaV_4S_8 and GeV_4S_8 were calculated with full-potential LAPW methods using the LDA + U approach. Both compounds undergo structural distortions from cubic to rhombohedral (GaV_4S_8) or orthorhombic (GeV_4S_8) symmetry at low temperatures. GaV_4S_8 is ferromagnetic below $T_C = 10$ K, whereas GeV_4S_8 shows antiferromagnetic order with $T_N = 13$ K. The spin structure of GeV_4S_8 was determined by neutron diffraction and described in the magnetic space group P_bmn2_1. The magnetic propagation vector is [$^1/_2$, $^1/_2$, 0] relating to the cubic paramagnetic unit cell. The LDA + U calculations ($U = 2$ eV) confirm the magnetic insulating ground states for the first time with magnetic moments and energy gaps in very good agreement with the experimental data. This method also reproduces the antiferromagnetic spin ordering of GeV_4S_8. The Jahn−Teller instability of the degenerated levels in the V_4 cluster MO drives the structural distortions, depending on the cluster electron count. Our results show how the interplay between the electronic, lattice, and spin degrees of freedom of the V_4 cluster units determines the physical and structural properties of these highly correlated transition-metal sulfides.

Introduction

Ternary chalcogenides with the *fcc* $GaMo_4S_8$ structure[1,2] represent an interesting class of highly correlated systems. Among representatives with niobium and tantalum, we have found transitions from Mott insulating to superconducting states under pressure and the absence of magnetic ordering in $GaNb_4S_8$ and related compounds.[3,4] In contrast, the vanadium sulfides AV_4S_8 (A = Ga, Ge) show no superconductivity, but ferro- or antiferromagnetism and structural instabilities at low temperatures.[5,6] The basic structure is built up by tetrahedral $(AS_4)^{n-}$ (A = Ga, $n = 5$; A = Ge, $n = 4$) and cubanelike $(V_4S_4)^{n+}$ units arranged in the NaCl manner. The vanadium atoms form tetrahedral V_4 clusters, with typical intracluster V−V distances of ∼2.8 Å, but long intercluster V···V distances of ∼4 Å. Both compounds are semiconductors because the valence electrons are localized in the cluster MOs. Electronic conduction takes place by hopping of carriers between the clusters,[7,8] and therefore we classify GaV_4S_8 and GeV_4S_8 as a new type of Mott insulators whose electronic properties depend on the special degrees of freedom of the cluster units. According to the ionic formula splitting $Ga^{3+}V_4^{3.25+}S_8^{2-}$ and $Ge^{4+}V_4^{3+}S_8^{2-}$, seven or eight valence electrons per V_4 cluster are available for metal−metal bonding, respectively. MO theory supplies six metal−metal bonding levels for a maximum cluster electron count of twelve. In the cubic case, the HOMO is 3-fold degenerate and occupied by one or two unpaired spins in GaV_4S_8 and GeV_4S_8, respectively. This prediction agrees with measurements of the magnetic susceptibilities, which revealed effective magnetic moments of 1.7 μ_B ($S = {}^1/_2$) and 2.8 μ_B ($S = 2/2$). The unpaired spins in GaV_4S_8 show ferromagnetic order below the Curie temperature $T_C = 10$ K, whereas an antiferromagnetic spin ordering was suggested for GeV_4S_8 below the Neél-temperature $T_N = 13$ K.[6] Electrical resistance measurements show semiconducting behavior with energy gaps of about 0.2 eV.

GaV_4S_8 undergoes a structural transition from cubic $F\bar{4}3m$ to rhombohedral $R3m$ symmetry (Figure 1) at $T_t = 38$ K, well above the onset of ferromagnetic ordering.[5] Thus far, GeV_4S_8 appeared to be cubic above the Neél temperature, but the spin structure has remained undetermined until now.

Apart from the unknown spin arrangement of GeV_4S_8 (the only antiferromagnetic $GaMo_4S_8$ type compound), the nature of the magnetic insulating ground states of the title compounds remains an open question. So far, all calculated electronic band structures proposed incorrect metallic ground states for $GaMo_4S_8$ type materials because the strong coulomb repulsion forces were not considered.[5,6,9,10] It has

* To whom correspondence should be addressed. E-mail: dirk.johrendt@cup.uni-muenchen.de.
† Ludwig-Maximilians-Universität München.
‡ CCLRC Rutherford Appleton Laboratory.

(1) Barz, H. *Mater. Res. Bull.* **1973**, *8*, 983.
(2) Perrin, C.; Chevrel, R.; Sergent, M. *C. R. Acad. Sci., Ser. C* **1975**, *280*, 949.
(3) Abd-Elmeguid, M. M.; Ni, B.; Khomskii, D. I.; Pocha, R.; Johrendt, D.; Wang, X.; Syassen, K. *Phys Rev. Lett.* **2004**, *93*, 126403.
(4) Pocha, R.; Johrendt, D.; Ni, B.; Abd-Elmeguid, M. M. *J. Am. Chem. Soc.* **2005**, *127*, 8732.
(5) Pocha, R.; Johrendt, D.; Pöttgen, R. *Chem. Mater.* **2000**, *12*, 2882.
(6) Johrendt, D. *Z. Anorg. Allg. Chem.* **1998**, *624*, 952.
(7) Sahoo, Y.; Rastogi, A. K. *J. Phys.: Condens. Matter* **1993**, *5*, 5933.
(8) Rastogi, A. K.; Niazi, A. *Physica B* **1996**, *223&224*, 588.
(9) Shanthi, N.; Sarma, D. D. *J. Solid State Chem.* **1999**, *148*, 143−149.
(10) Le Beuze, A.; Loirat, H.; Zerrouki, M. C.; Lissillour, R. *J. Solid State Chem.* **1995**, *120*, 80.

10.1021/cm052809m CCC: $33.50
Published on Web 03/28/2006

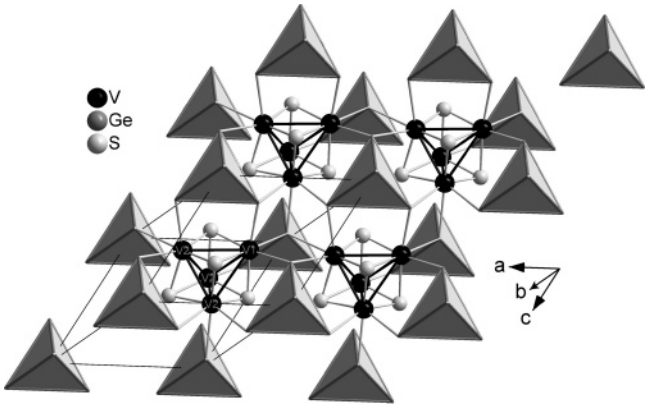

Figure 1. Crystal structure of LT-GaV_4S_8 below 38 K (space group *R*3*m*, rhombohedral axes). The $(V_4S_4)^{5+}$ cluster units and the $(GaS_4)^{5-}$ tetrahedra are emphasized.

therefore been a challenging effort to establish a physically correct description of the electronic structure of these highly correlated cluster systems.

In the present paper, we present calculated electronic structures of Mott insulators GaV_4S_8 and GeV_4S_8, which are for the first time in agreement with the magnetic insulating properties. We have used the LDA + *U* method to calculate the band structures of these compounds. In the case of GeV_4S_8, we also report the spin structure of the low-temperature modification determined by neutron powder diffraction.

Experimental Section

Electronic Band Structure Calculations. Self-consistent electronic structure calculations were performed with the WIEN2k program package[11,12] using density functional theory (DFT) within the full-potential LAPW method and the local density approximation (LDA) method. Full-potential LAPW is based on the muffin-tin construction with nonoverlapping spheres. Within these spheres of radius $r_{mt,\alpha}$ (α = atom type), the angular dependence of the potential $V_\alpha(r)$ is expanded in spherical harmonics $V_\alpha(r) = \sum_{lm_l} V_{\alpha lm_l}(r) Y_l^{m_l}(\hat{r})$ for $r < r_{mt,\alpha}$. In the interstitial region between the spheres, the potential is represented by a plane wave expansion $V(r) = \sum_{K_n} V_{K_n} e^{iK_n r}$, with K_n being the reciprocal lattice vectors. Because of the great flexibility and accuracy of this expansion for the potential and charge density, a very high numerical accuracy is achieved for the LAPW method. Mixed LAPW and APW + *lo* (*lo* = local orbitals) basis sets were used to increase the efficiency of the APW linearization.[13,14] Further technical details can be found in ref 12 and the monograph of Singh.[15]

The total energies and charge densities of the SCF cycles converged to changes smaller than 1×10^{-4} Ryd cell^{-1}. The basis sets consisted of 2311 or 6967 plane waves for GaV_4S_8 and GeV_4S_8, respectively, up to a cutoff $R_{mt}K_{max} = 8.0$. The atomic sphere radii R_{mt} were 1.9 (Ga, Ge), 2.3 (V), and 1.8 au (S); 570 *k*-points (GaV_4S_8, 18 × 18 × 18 mesh) or 12 *k*-points (AFM-GeV_4S_8, 5 × 2 × 3 mesh) were used in the irreducible wedges of the Brillouin zones.

To calculate the magnetic insulating ground states, we have used the LDA + *U* approach[16] with the SIC method for double counting correction,[17] as implemented in the WIEN2k program. A value of 2 eV was used for the effective Hubbard *U* (*J* = 0), which makes the energy of a level ϵ_i dependent on its degree of occupation n_i, according to $\epsilon_i = \epsilon_{i,LDA} + U(^1/_2 - n_i)$. The antiferromagnetic state of orthorhombic GeV_4S_8 was achieved by a constrained calculation, where the spin ↑ and spin ↓ sublattices were connected by the magnetic propagation vector (0, $^1/_2$, 0).

Neutron Diffraction. Neutron powder diffraction data were collected on GeV_4S_8 on the time-of-flight diffractometer ROTAX at the ISIS Facility, Rutherford Appleton Laboratory, U.K. A powder sample of about 4 g was loaded into a cylindrical vanadium container of 8 mm diameter, which was then mounted in a 4 K closed-cycle refrigeration cryostat. The sample container was wrapped with the cold surface of the cryostat in aluminum foil in order to decrease the heat load via thermal radiation. The neutron beam height was 30 mm. Data were collected using three fixed-angle position-sensitive scintillation detectors, centered at scattering angles of 28.9, 89.5, and 158 degrees, yielding three diffraction patterns covering different *d* spacing regions. Neutron data were acquired for 8 h at 4 and 300 K, and for 1 h at temperatures between 4 and 30 K. The crystal and magnetic structure parameters were determined using the GSAS suite of programs.[18] The Rietveld refinements included all three diffraction patterns, where the forward scattering data (28.9 degrees) typically contain the magnetic Bragg peaks and the backscattering data cover the *d* spacing range from 0.3 to 2.5 Å in best resolution.[19] The neutron scattering lengths used were ($\times 10^{-12}$ cm) 0.818 (Ge), 0.038 (V), and 0.285 (S). In refinements of the magnetic moment, the magnetic form factor for V^{3+} was calculated for a spherical $\langle j0 \rangle$ form factor expansion as implemented in the GSAS program, with coefficient taken from ref 20. The time-of-flight peak shape parameters were fitted by double-exponential-pseudo Voigt functions provided by GSAS as profile shape function no. 3. The background for each the three neutron-diffraction patterns was modeled using 8th order Chebyschev polynomials. An empirical absorption parameter for the wavelength-specific absorption of neutrons by the sample was refined. Weak Bragg peaks originating from the aluminum foil were modeled as a second phase in the Rietveld analysis.

Results and Discussion

Ferromagnetic GaV_4S_8. Because some general electronic and crystallographic features of GaV_4S_8 are already known,[1,21] we focus our discussion of the electronic structure with regard to the properties as a ferromagnetic Mott insulator. As we reported earlier, GaV_4S_8 undergoes a structural phase transition from the cubic room-temperature phase (space group $F\bar{4}3m$) to the rhombohedral low-temperature phase

(11) Blaha, P.; Schwarz, K.; Madsen, G. K. H.; Kvasnicka, D.; Luitz, J. *WIEN2k: An Augmented Plane Wave + Local Orbitals Program for Calculating Crystal Properties*; TU Wien: Vienna, Austria, 2001.
(12) Schwarz, K.; Blaha, P. *Comput. Mater. Sci.* **2003**, *28*, 259.
(13) Sjostedt, E.; Nordstrom, L.; Singh, D. J. *Solid State Commun.* **2000**, *114*, 15−20.
(14) Madsen, G. K. H.; Blaha, P.; Schwarz, K.; Sjostedt, E.; Nordstrom, L. *Phys. Rev. B* **2001**, *64*, 195134/1−195134/9.
(15) Singh, D. J.; Nordstrom, L. *Planewaves, Pseudopotentials and the LAPW Method*; Springer: New York, 2006.
(16) Anisimov, V. I.; Aryasetiawan, F.; Lichtenstein, A. I. *J. Phys.: Condens. Matter* **1997**, *9*, 767−808.
(17) Anisimov, V. I.; Solovyev, I. V.; Korotin, M. A.; Czyzyk, M. T.; Sawatzky, G. A. *Phys. Rev. B* **1993**, *48*, 16929−34.
(18) Larson, A. C.; von Dreele, R. B. *GSAS: General Structure Analysis System*; Los Alamos Laboratory Report LAUR; Los Alamos National Laboratory: Los Alamos, NM, 2004.
(19) Kockelmann, W.; Weisser, M.; Heinen, H.; Kirfel, A.; Schäfer, W. *Mater. Sci. Forum* **2000**, *321−324*, 332.
(20) Brown, P. J. *Magnetic Form Factors, International Tables for Crystallography, Vol. C*; Wilson, A. J. C., Ed.; Kluwer Academic Publishers: Dordrecht, The Netherlands, 1995; p 391.

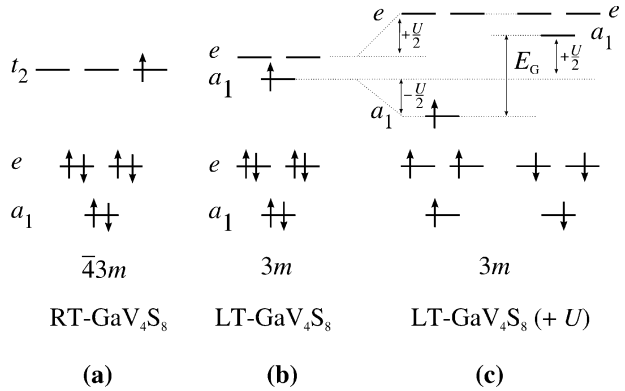

Figure 2. Molecular orbital (MO) schemes of V_4 cluster units in GaV_4S_8, occupied with seven electrons. (a) cubic $\bar{4}3m$, (b) trigonal $3m$, and (c) trigonal $3m$ spin-polarized with U.

($LT\text{-}GaV_4S_8$, space group $R3m$) at $T_t = 38$ K. This transition removes the 3-fold degeneracy of the HOMO ($\bar{4}3m$ symmetry), which splits to one lower a_1 and a 2-fold degenerated e level ($3m$ symmetry), as depicted in panels a and b of Figure 2. Nonetheless, conventional spin-polarized calculations with LDA or GGA functionals resulted in metallic ground states, because the splitting between the a_1 and e orbitals due to distortion alone is smaller than the width of the band generated by the a_1 level. Thus, the Fermi energy cuts the a_1 band and feigns the incorrect metallic state. Figure 2c illustrates the effect of U schematically. The energy ϵ_i of the ith level becomes dependent from its occupation n_i by the amount $\Delta\epsilon_i = U(^1/_2 - n_i)$. Thus, the LDA orbital energies are expected to shift by $-U/2$ for occupied ($n_i = 1$) and $+U/2$ for unoccupied orbitals ($n_i = 0$).

Within density functional theory (DFT) calculations, the choice of the effective U value to correct the LDA energies is still under discussion. Traditionally, U is treated in LDA + U as an adjustable parameter in order to achieve agreement with experimental data like magnetic moments and band-gap values. Meanwhile, procedures are available to calculate effective U values ab initio within the DFT formalism.[22] To approximate a U for GeV_4S_8, we used the method recently described by Madsen and Novák,[23] assuming the oxidation state of vanadium to be V^{3+}. Calculations with constrained 3d electron configurations ($(n + 1)/2\uparrow$, $n/2\downarrow$) and ($(n + 1)/2\uparrow$, $(n/2) - 1\downarrow$) ($n = 2$), treated as unhybridized core states, resulted in a U of ~3 eV. Spin-polarized LDA + U calculations of the $LT\text{-}GaV_4S_8$ using $U = 3$ eV and $R3m$ symmetry revealed, however, magnetic moment values that were too large compared with the experimental value of one spin per V_4. We found that an effective U of 2 eV is already sufficient to reproduce the physical properties of GaV_4S_8, in good agreement with the experimental data. The calculated magnetic moment corresponds to almost exactly one spin per V_4 cluster ($S = 1/2$), and an insulating gap of $E_G = 0.14$ eV occurs above the Fermi level. It is generally accepted that the correct magnetic moment is a fundamental test for the LDA + U functional, whereas a rigorous band gap requires further corrections.[24] However, our calculations

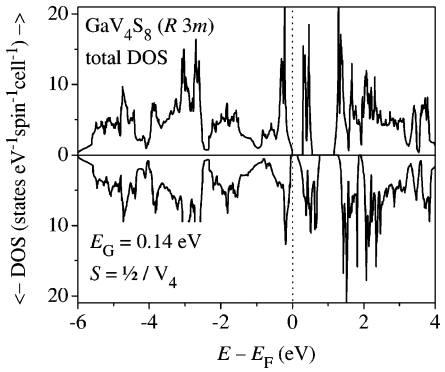

Figure 3. Spin-polarized density of states of GaV_4S_8 (space group $R3m$) calculated with the LDA + U method ($U = 2$ eV). The energy zero is taken at the Fermi level.

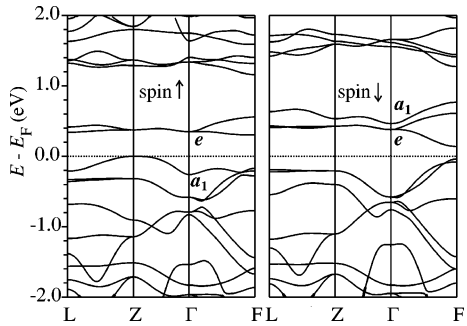

Figure 4. Band dispersions of GaV_4S_8 (space group $R3m$), calculated with the LDA + U method and $U = 2$ eV. The bands of the majority (left) and minority (right) spin are plotted along the symmetry lines $L(0,^1/_2,0) \rightarrow Z(^1/_2,^1/_2,^1/_2) \rightarrow G(0,0,0) \rightarrow F(0,^1/_2,^1/_2)$. The labels e and a_1 refer to the Γ point (symmetry $3m$) and correspond to the levels given in the MO scheme in Figure 2.

reproduce the exact magnetic (spin) moment and a band gap that is not too far from the experimental value.

The spin-polarized LDA + U density-of-states of rhombohedral $LT\text{-}GaV_4S_8$ is shown in Figure 3. As expected from the MO scheme in Figure 2, the band gap occurs within the initially 3-fold degenerated t_2 HOMO, which splits first by symmetry lowering into one a_1 and a 2-fold degenerated e level. But the spin-polarized calculation places the empty $a_1\downarrow$ level above the empty $e\downarrow$ levels and thus the insulating gap occurs not between $a_1\uparrow$ and $a_1\downarrow$, but between $a_1\uparrow$ and $e\downarrow$. This also becomes evident from the band structure pictures shown in Figure 4. The strong splitting of the $a_1\uparrow$ and $a_1\downarrow$ bands[25] is clearly discernible, and the small indirect band gap opens between the $a_1\uparrow$ and $e\downarrow$ bands at the Z and F points in the Brillouin zone, respectively.

A closer inspection of the eigenvalues of the bands reveals that the occupied $a_1\uparrow$ states contain much more contributions from the apical V1 atom than from the basal V2. This also becomes evident from the spin-polarized partial DOS of the vanadium $3dz^2$ orbitals (a_1), which are depicted in Figure 5. It is clearly seen that the $3dz^2\uparrow$ of the V1 atom is completely filled, whereas the corresponding $3dz^2\downarrow$ is well above E_F (shaded areas), but for the V2 atoms, the $3dz^2\uparrow$ and $3dz^2\downarrow$

(21) Shanti, N.; Sarma, D. D. *J. Solid State Chem.* **1999**, *148*, 143.
(22) Anisimov, V. I.; Gunnarsson, O. *Phys. Rev. B* **1991**, *43*, 7570.
(23) Madsen, G. K. H.; Novák, P. *Europhys. Lett.* **2005**, *69*, 777.
(24) Shick, A. B.; Liechtenstein, A. I.; Pickett, W. E. *Phys. Rev. B* **1999**, *60*, 10763.
(25) The symmetry labels a_1 and e are valid only for the band states at the Γ point, where the point group is $3m$ (as for the molecular model). For clarity, we use the term a_1 and e also for those band states that are developed by these orbitals, even though they obey not the point group $3m$.

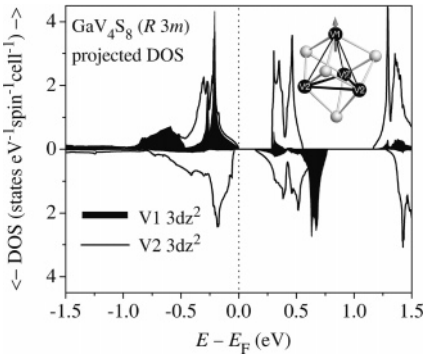

Figure 5. Partial DOS of the $3dz^2$ orbitals of V1 (shaded area) and V2 (lines) in LT-GaV_4S_8. The Fermi level clearly separates the $3dz^2$ ↑ and $3dz^2$ ↓ of the V1 atoms, which places the most part of the spin ↑ density at the V1 atom (insert).

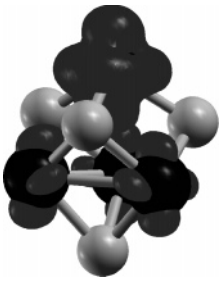

Figure 6. Calculated spin density in the V_4S_4 cubes of GaV_4S_8.

are both partially filled. This means that the unpaired majority spin ↑ density is essentially located at the V1 atom, whereas the three V2 atoms remain almost nonmagnetic. This at first glance peculiar result can also be explained by considering the chemical bonding within the V_4 cluster. The orbital overlap of the apical $3dz^2$ (V1) with the basal $3dz^2$ (V2) depends on the rhombohedral angle α_{rh}.[5] Smaller α_{rh} values (<60°) increase the bonding overlap and lower the energy of the a_1 orbital. Consequently, the stronger bonding $3dz^2$ (V1) orbital coefficient increases, and because this orbital is occupied by spin ↑ electrons, we find most of the spin density located at V1. In terms of the calculated magnetic moments, we calculate 0.696 spins located inside the V1 sphere, 0.070 in the V2 sphere, and 0.117 spins in the interstitial. The latter can be considered as a spin-density leakage of the muffin-tin sphere of V1 and can safely be added to this atom. Our calculated magnetic moment is then $0.696 + (3 \times 0.07) + 0.117 = 1.023$ unpaired spins per V_4 cluster, in excellent agreement with the magnetic measurements. The corresponding spatial distribution of spin density within the $(V_4S_4)^{5+}$ cubes is depicted in Figure 6 and further illustrates the localization of the one unpaired spin at the "top" of the V_4 cluster. However, this at first glance unexpected spin ordering is not verified by experimental data at this time. We believe, nonetheless, that this result is by no means an artifact of the calculation, and the following section on GeV_4S_8 will support this viewpoint.

Antiferromagnetic (AFM) GeV_4S_8. The structure of GeV_4S_8 at room temperature is *fcc* cubic and isotypic to GaV_4S_8. The main difference is the occupation of the cluster MO with eight instead of seven electrons according to $Ge^{4+}V_4^{3+}S_8^{2-}$. Magnetic measurements verified the presence of two unpaired spins per V_4 cluster in GeV_4S_8 ($\mu_{eff} = 2.83$ μ_B) and also indicated antiferromagnetic ordering below T_N = 13 K.[6] We have already discussed some properties of the electronic structure and chemical bonding of GeV_4S_8 in ref 6. In those days, we pointed out that a physically correct antiferromagnetic insulating ground state could only be achieved if (i) the antiferromagnetic spin structure of GeV_4S_8 is known and (ii) the coulomb repulsion would be considered in the LDA calculations. We have performed neutron powder diffraction on GeV_4S_8 to determine the microscopic spin structure.

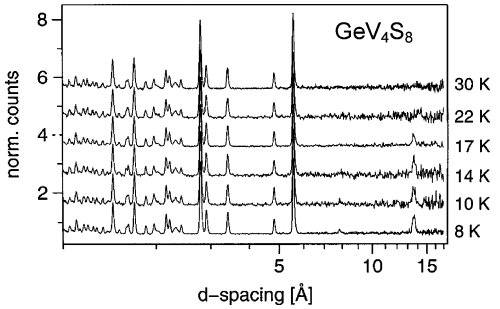

Figure 7. Forward neutron-scattering patterns of GeV_4S_8 at low temperatures.

Vanadium nuclei as constituents of the crystal structure have almost zero scattering power for neutrons. On the other hand, the magnetic moments located at the V sites are visible for neutrons through magnetic interaction with the magnetic moment of the probe. A series of patterns with decreasing temperature is shown in Figure 7, where the appearance of an additional magnetic reflection starting from 22 K is clearly discernible at d = 13.6 Å. A closer inspection revealed further weak magnetic peaks at d = 7.8 and 5.1 Å. Indexing with respect to the original cubic cell with a_c = 9.655 Å results in a noninteger *hkl* of ($^1/_2$ $^1/_2$ 0) for the first, ($^1/_2$ $^1/_2$ 1) for the second, and ($^3/_2$ $^1/_2$ 1) for the third peak. Thus, the magnetic propagation vector is [$^1/_2$, $^1/_2$, 0]. The periodicity of the magnetic moment modulation in real space is thus $a_c\sqrt{2}$ = 13.654 Å, and all magnetic peaks may then be indexed with a tetragonal magnetic cell $a_{m,t}$ = 13.654 Å and $c_{m,t}$ = 9.655 Å as (1 0 0), (1 0 1), and (2 1 1). If so, the underlying nuclear (chemical) structure may be described as tetragonal with $a_{n,t}$ = 6.827 Å and $c_{n,t}$ = 9.655 Å in space group $I\bar{4}m2$ (group−subgroup relation $F\bar{4}3m \xrightarrow{t_3} I\bar{4}m2$). The antiferromagnetic ordering should then double the $a_{n,t}$ axis. However, first attempts to refine the nuclear scattering data collected at 4 K with this tetragonal model were not successful, because some reflections show a small but distinct splitting that is incompatible with a tetragonal lattice. As an example, a reflection at d = 2.78 Å is clearly split in two peaks, whereas the tetragonal cell allows symmetry-equivalent reflections (2 0 2) ≡ (0 2 2) at this position. Thus, the symmetry of the chemical structure at 4 K has to be further reduced to the orthorhombic space group *Imm*2 ($I\bar{4}m2 \xrightarrow{t_2} Imm2$). From this, we infer that the magnetic propagation can be described by one component, by doubling either the orthorhombic $a_{n,o}$ or $b_{n,o}$ axis of the chemical cell. Rietveld refinements of the nuclear scattering using the *Imm*2 orthorhombic model gave small residuals and lattice parameters of $a_{n,o}$ = 6.8362(2) Å, $b_{n,o}$ = 6.79345(3) Å, and $c_{n,o}$ = 9.6384(4) Å. The next step was to construct a model for the

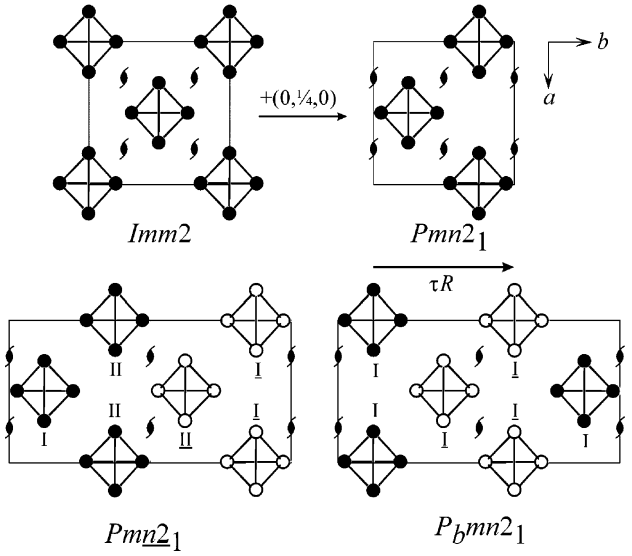

Figure 8. Construction of the antiferromagnetic spin structure in GeV_4S_8, starting from the low-temperature chemical structure in space group *Imm*2. Only the V_4 cluster units are depicted as black (spin ↑) and white (spin ↓) spheres. The 2_1 screw axes are depicted to emphasize the relations between the space groups.

magnetic structure. The magnetic space group of paramagnetic GeV_4S_8 is the ordinary Fedorov group *Imm*2 or, if time reversal *R* is included, the gray group *Imm*2$\underline{1}$. A model of the antiferromagnetic spin structure may be constructed from symmetry considerations, as illustrated in Figure 8. First, the body centering is lost in the antiferromagnetic phase because of the doubling of the unit cell. We therefore looked for a subgroup of *Imm*2 on the basis of a primitive Bravais lattice before introducing the time reversal operator *R* and before carrying out the unit-cell doubling. By shifting the origin of the chemical *Imm*2 unit cell by $(0,^1/_4,0)$, the space-group symmetry is reduced to $Pmn2_1$. The additional translation τR then doubles the $b_{n,o}$ axis to b_m and leads to the magnetic space group $Pmn\underline{2}_1$ with an uncolored or, when the origin is shifted by $-(0,^1/_4,0)$, to P_bmn2_1 with a colored Bravais lattice.[26]

For these magnetic models, the first and strongest magnetic reflection is indexed as (0 1 0). Hence, one can assume that the main components of the magnetic moment vectors are perpendicular to the b_m axis. For simplicity, we use a spin orientation parallel to the polar c_m axis, i.e., alignments along [0 0 1] for spin ↑ and [0 0 $\bar{1}$] for spin ↓. To minimize the number of parameters in the refinements, we initially distributed the experimental magnetic moment equally over the V_4 cluster, i.e., assigned $^1/_4$ μ_B to each vanadium atom. Refinements with both models (Figure 8) produced the magnetic reflections with almost identical residuals. Hence the two proposed space groups are not distinguishable within the accuracy of our diffraction data. The two models differ in that there are two crystallographically different V_4 clusters (I and II in Figure 8) in $Pmn\underline{2}_1$ with the 2_1 screw axis as an antisymmetry operation, whereas only one type of V_4 cluster exists in P_bmn2_1 with a normal 2_1 screw and the anti-translation $\tau R = (0, ^1/_2, 0)$ as the only antisymmetry operation. First refinements in the magnetic space group P_bmn2_1 kept equal magnetic moments on every cluster atom, with calculated magnetic intensities agreeing reasonably well with observed intensities. However, the disband of this moment constraint leads to a much better fit of the diffraction patterns. Final least-squares cycles converged to $R_p = 0.027$ and $R_F = 0.031$ and magnetic moments of 0.697(5) μ_B at V1 and 0.128(6) μ_B at V2 and V3. The resulting total magnetic moment of 1.65 μ_B per V_4 cluster is somewhat smaller than expected (2 μ_B). However, one must keep in mind that the neutron data did not allow for refinement of the magnetic moment orientation, the moment were assumed to be aligned parallel [0 0 1]. Besides that, it should be noted that we observed a slightly higher slope of the Curie−Weiss fit at lower temperatures,[6] indicating a slightly smaller magnetic moment per V_4 cluster of ~1.8 μ_B per V_4, which is in better agreement with the neutron-diffraction data.

(26) Opechowski, W.; Guccione, R. Magnetic Symmetry. In *Magnetism*; Rado, G. T., Suhl, H., Eds.; Academic Press: New York, 1963; Vol. IIa, p 136.

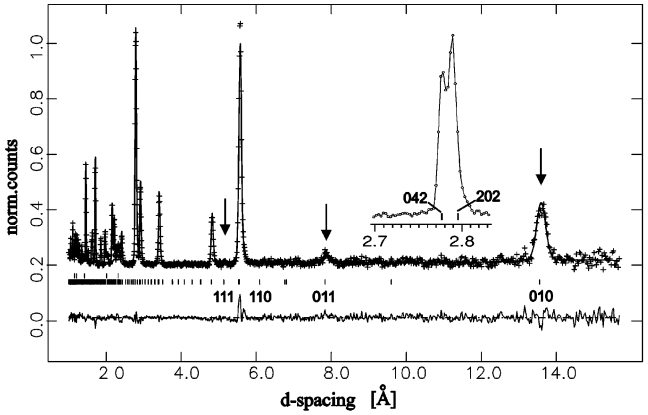

Figure 9. Neutron-scattering pattern and Rietveld fit of AFM-GeV_4S_8 at 4 K. Arrows indicate magnetic Bragg peaks. The insert highlights the *d* spacing range around $d = 2.8$ Å where the nuclear peak splitting is clearly visible.

Table 1. Rietveld Refinement of Crystal and Magnetic Structure Parameters of AFM-GeV_4S_8 at 4 K

empirical formula	GeV_4S_8
magnetic space group	P_bmn2_1
fw (g mol^{-1})	532.87
T (K)	4
a_m (Å)	6.8362(2)
b_m (Å)	13.587(1)
c_m (Å)	9.6384(4)
V (Å^3)	895.25(4)
Z	4
d_{calcd} (g cm^{-3})	3.953
no. of data points	4901
no. of reflns	1139
no. of variable atomic params	32
no. of variable profile params	17
d range	$1.0 < d < 15.7$
R_p, wR_p	0.0259, 0.0309
R_F, χ^2	0.0585, 3.885

A section of the profile-fitted neutron-diffraction pattern at 4 K is shown in Figure 9. Refined structural parameters obtained from combined nuclear and magnetic Rietveld refinements are compiled in Tables 1 and 2. Selected atomic distances are given in Table 3. Figure 10 depicts the magnetic orthorhombic unit cell of AFM-GeV_4S_8 with the main spin components emphasized as arrows.

The cubic $\bar{4}3m$ symmetry of the V_4S_4 units is lowered to *mm*2 in AFM-GeV_4S_8 (see Figure 11). But in contrast to LT-GaV_4S_8 described above, this structural distortion is now

Table 2. Atomic Positions of Antiferromagnetic GeV_4S_8 at 4 K, Magnetic Space group P_bmn2_1

atom	Wyckoff position[a]	*x*	*y*	*z*	μ/μ_B
V1	4*b* (*x*, *y*, *z*)	0.2878(9)	0.1243(6)	0.1047(9)	0.697(5)
V2	2*a* (0, *y*, *z*)	0.0000	0.9724(7)	0.3841(4)	0.128(6)
V3	2*a* (0, *y*, *z*)	0.0000	0.7738(7)	0.3888(6)	0.128(6)
Ge	2*a* (0, *y*, *z*)	0.0000	0.3756(8)	0.9968(6)	
S1	2*a* (0, *y*, *z*)	0.0000	0.0143(1)	0.1288(8)	
S2	4*b* (*x*, *y*, *z*)	0.2366(3)	0.1316(5)	0.8712(3)	
S3	4*b* (*x*, *y*, *z*)	0.2703(1)	0.8760(9)	0.8675(3)	
S4	2*a* (0, *y*, *z*)	0.0000	0.2405(3)	0.1339(5)	
S5	2*a* (0, *y*, *z*)	0.0000	0.0042(5)	0.6313(1)	
S6	2*a* (0, *y*, *z*)	0.0000	0.2454(4)	0.6323(4)	

[a] Only coordinates of the spin ↑ atoms are given, coordinates of the spin ↓ atoms result by adding $R = [0, {}^1/_2, 0]$.

Table 3. Interatomic Distances in AFM-GeV_4S_8 (Å ± 0.005)[a]

V1−S2	2.280	V2−S2	2.292	V3−S2	2.219
V1−S5	2.284	V2−S2	2.292	V3−S2	2.219
V1−S6$^+$	2.304	V2−S5	2.422	V3−S6$^+$	2.379
V1−S1	2.482	V2−S1	2.526	V3−S6	2.498
V1−S4	2.538	V2−S3	2.595	V3−S3$^+$	2.579
V1−S3	2.564	V2−S3	2.595	V3−S3$^+$	2.579
V1−V2	2.889	V2−V3	2.699	V3−V2	2.699
V1−V3	2.889	V2−V1	2.889	V3−V1	2.889
V1−V1	2.901	V2−V1	2.889	V3−V1	2.889
V1−V2	3.922	V2−V1	3.922	V3−V1$^+$	3.936
V1−V1	3.935	V2−V1	3.922	V3−V1$^+$	3.936
V1−V3$^+$	3.936	V2−V3$^+$	4.095	V3−V2$^+$	4.095
Ge−S3$^+$	2.229				
Ge−S3$^+$	2.229				
Ge−S4	2.262				
Ge−S1$^+$	2.274				

[a] Atomic positions marked with + are generated by the additional translation $[0, {}^1/_2, 0]$.

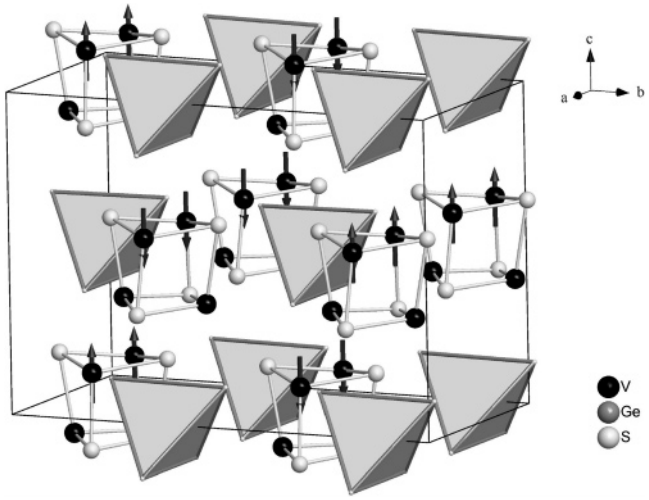

Figure 10. Magnetic unit cell of GeV_4S_8, space group P_bmn2_1. Arrows symbolize the main contribution of the magnetic moment located at V1.

directly connected with the onset of antiferromagnetic ordering, whereas the structural transition in GaV_4S_8 occurs well above the ferromagnetic Curie temperature. A look at the atomic distances within the cluster shows that one of the six V−V bonds is considerably shortened (∼2.7 Å) and the other five are much longer (∼2.9 Å) now. The sulfur coordination around the V-atoms is also distorted because of the reduction of the site symmetry from 3*m* to *mm*2. In terms of the cluster MO model, this distortion removes the 3-fold degeneracy of the HOMO and enables the formation of an energy gap. Because the point group *mm*2 contains

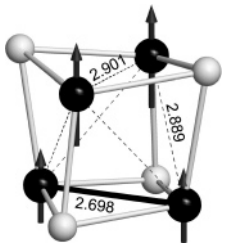

Figure 11. V_4S_4 unit with *mm*2 symmetry in magnetically ordered GeV_4S_8. Arrows symbolize the magnetic moments of 0.697 μ_B at V1 and 0.128 μ_B at V2 and V3.

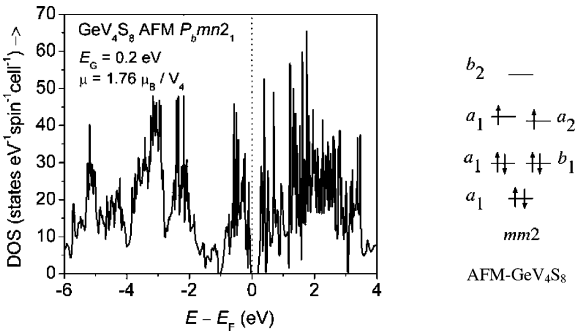

Figure 12. Total density of states of AFM-GeV_4S_8 (left) and the MO scheme of the V_4 cluster with *mm*2 symmetry occupied by eight electrons (right).

only one-dimensional representations, there are no degenerated levels. The magnetic moment is mainly located on the V1 atoms, which form quasi-one-dimensional chains of ferromagnetically ordered atoms running along [100]. These chains themselves are antiferromagnetically modulated along [010] by the magnetic propagation vector $[0, {}^1/_2, 0]$, as shown in Figure 10.

This model of the spin structure of AFM-GeV_4S_8 was used for the following LDA + *U* calculations in the space group $Pmn2_1$. A special routine automatically inverts the spin components of all atoms connected by the propagation vector $[0, {}^1/_2, 0]$. The resulting density-of-states is shown in Figure 12. A gap of ∼0.2 eV is discerned at the Fermi level; thus, for the first time, a magnetic insulating ground state of GeV_4S_8 is found to agree with the physical properties. Also, the theoretical magnetic moments are in good agreement with the experimental neutron-diffraction data. We find 0.762 μ_B at V1 (exp: 0.697(5)) and 0.117 μ_B at V2 and V3 (exp: 0.128(6)).

The results of the antiferromagnetic (AFM) calculation were checked against the ferromagnetic (FM) solution. Table 4 shows total energies, magnetic moments, and energy gaps of GeV_4S_8. The benefits of the LDA + *U* method are clearly seen. The AFM solution with LDA + *U* lies about 12 mRyd (0.163 eV) below the FM result, whereas the LDA predicts the FM state to be more stable. The LDA + *U* magnetic moments are in better agreement with the experimental data. Satisfactory energy gaps occur in the AFM and FM case, but the magnetic moments of the latter are implausible.

The localization of the magnetic moments on the V1 atoms with weaker V−V bonds as found from the neutron data is also well predicted by the LDA + *U* calculation. The corresponding spin-density distribution within the V_4S_4 units is depicted in Figure 13. Extrapolating from this result on

Table 4. Comparison of the Ferro-/Antiferromagnetic LDA and LDA + *U* Solutions of GeV_4S_8

	LDA	LDA + *U*	exp
	AFM-GeV_4S_8		
E_{total} (Ryd)	−18140.592732	−18140.057462	
$\mu_{cluster}$ (μ_B)	1.474	1.758	1.650−2.0[a]
μ_{V1} (μ_B)	0.569	0.756	0.697(5)
μ_{V2V3} (μ_B)	0.168	0.123	0.128(6)
E_{gap} (eV)	0	0.2	0.2
	FM-GeV_4S_8		
E_{total} (Ryd)	−18140.618414	−18140.044919	
$\mu_{cluster}$ (μ_B)	1.735	2.094	
μ_{V1} (μ_B)	0.645	1.017	
μ_{V2} (μ_B)	0.222	−0.033	
E_{gap} (eV)	0	0.2	

[a] 2 μ_B from magnetic susceptibility measurements.

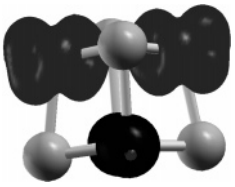

Figure 13. LDA + *U* spin density within the V_4S_4 unit of AFM-GeV_4S_8.

GeV_4S_8, we justify the localization of the magnetic moment on the one apical V atom in GaV_4S_8.

The relatively large unit cell and the low symmetry preclude detailed discussions on the band structure of AFM-GeV_4S_8. However, the inspection of the eigenvalues at the Γ point shows again that the energy gap arises by lifting the 3-fold degeneracy of the HOMO, as schematically depicted in Figure 12 (right). Two spins remain unpaired, and antiferromagnetic ordering occurs between the neighboring clusters at low temperatures.

Apparently, these Jahn−Teller distortions as found in GaV_4S_8 with seven electrons and in GeV_4S_8 with eight electrons per V_4 cluster constitute the driving force for the structural distortions. We believe that the reduction of symmetry is an important precondition for the formation of an energy gap, the localization of the magnetic moments, and the long-range magnetic ordering. In the case of GaV_4S_8, the structural and magnetic phase transitions occur at well-separated temperatures (T_f = 38 K, T_C = 10 K). So far, we could not find experimental evidence that the structural transition of GeV_4S_8 takes place well above the antiferromagnetic Neél temperature. Therefore, the Peierls distortion is assumed to occur just above or even simultaneously with the onset of the antiferromagnetic ordering in GeV_4S_8.

Conclusion

The magnetically ordered insulating ground states of Mott insulators GaV_4S_8 and GeV_4S_8 originate from the Jahn−Teller instability of the tetrahedral V_4 cluster units. The nature of the structural distortion depends on the cluster electron count and can be rationalized by a simple MO scheme. One unpaired spin in the 3-fold degenerated HOMO as in GaV_4S_8 leads to a rhombohedral distortion (3*m*); two unpaired spins in GeV_4S_8 result in orthorhombic symmetry (*mm*2) of the V_4 cluster units. Ferromagnetic ordering of the cluster moments occurs in GaV_4S_8, whereas we find a rather complex antiferromagnetic spin structure in GeV_4S_8. The quantum chemical calculations with the LDA + *U* approach reproduce the ground states of both compounds in good agreement with experimental data and confirm the accumulation of the unpaired ordered spin density on one or two V atoms of the V_4 cluster, whereas the remaining vanadium atoms are almost nonmagnetic. One may consider this as a kind of charge ordering according to V^{2+} forming V−V bonds and two magnetic V^{4+} (d^1) species. This is reminiscent of the well-known Verwey transition in Fe_3O_4,[27] where the underlying pyrochlore network of iron ions shows a similar ordering scheme of Fe^{2+} and Fe^{3+} aligned into chains.[28]

Our results show that the interplay between the electronic, lattice, and spin degrees of freedom of the V_4 cluster units determines the physical and structural properties of these highly correlated transition-metal sulfides. It is remarkable that the localization of electrons in the cluster MO occurring at low temperatures forces rather complicated structural distortions and/or magnetic ordering patterns. Furthermore, it appears satisfactory that the LDA + *U* approach is able to describe even these complex systems in good agreement with experimental data.

Acknowledgment. This work was financially supported by the Deutsche Forschungsgemeinschaft (Project Jo257-2/2).

CM052809M

(27) Walz, F. *J. Phys.: Condens. Matter* **2002**, *14*, R285.
(28) Bickford, L. R. *Rev. Mod. Phys*. **1953**, *25*, 75.